# Non-destructive screening methodology based on handheld XRF for the classification of concrete

## cement type-driven separation

Nedeljković, Marija; Tošić, Nikola; Holthuizen, Patrick; França de Mendonça Filho, Fernando; Copuroglu, Oguzhan; Schlangen, Erik; Fennis, Sonja

**DOI**
10.1617/s11527-023-02147-3

**Publication date**
2023

**Document Version**
Final published version

**Published in**
Materials and Structures

**Citation (APA)**
Nedeljković, M., Tošić, N., Holthuizen, P., França de Mendonça Filho, F., Copuroglu, O., Schlangen, E., & Fennis, S. (2023). Non-destructive screening methodology based on handheld XRF for the classification of concrete: cement type-driven separation. *Materials and Structures*, *56*(3), Article 54. https://doi.org/10.1617/s11527-023-02147-3

Materials and Structures (2023)56:54
https://doi.org/10.1617/s11527-023-02147-3

ORIGINAL ARTICLE

# Non-destructive screening methodology based on handheld XRF for the classification of concrete: cement type-driven separation

**Marija Nedeljković · Nikola Tošić · Patrick Holthuizen · Fernando França de Mendonça Filho · Oğuzhan Çopuroğlu · Erik Schlangen · Sonja Fennis**

Received: 15 September 2022 / Accepted: 7 March 2023


**Abstract** The utilization of locally available concrete waste for producing recycled concrete aggregates is recognized as one of the most sustainable ways of satisfying the growing demand for concrete production. However, the quality of concrete waste depends on its origin and it may significantly differ from one concrete structure to another. Knowing the chemical composition of the parent concrete is crucial for determining or verifying the origin of the raw materials. For this reason, pre-demolition concrete waste streams need to be characterized and classified. Therefore, a new non-destructive method for determining the cement and aggregate type in hardened concrete using handheld X-ray fluorescence (hXRF) analyser is presented in this paper. The method was tested on different raw powders and on concretes containing different types of cements including CEM I 42.5 N (Portland cement), CEM II/B-V 42.5 N (Portland-fly ash cement), CEM III/B 42.5 N (GGBFS cement). Combined desktop XRF and Energy-dispersive X-ray Spectroscopy (EDS) measurements were used for the purpose of validation. The results revealed that the curing of concrete affects the results: a dried concrete surface condition was optimal for measurements since it limits the impact of the concrete surface moisture and efflorescence on characteristic element oxides, such as CaO. The effective measurement duration was 30 s. A CEM III/B 42.5 N (GGBFS)-based concrete surface was distinguished from other concretes using $Al_2O_3$, MgO and $Fe_2O_3$ as characteristic oxides. The inner layers of concrete were rich in $SiO_2$, the oxide characteristic for the aggregate composition tested in this study. This shows that hXRF is suitable for use in concrete, provided that the concrete surface is dried and the characteristic elements are defined to ensure a distinction between different cement and aggregate types. Direct adoption of such characterization, however, requires field testing across a wide range of concrete compositions and in situ conditions.

**Keywords** Cement · Aggregate · Concrete · Surface analysis · Chemical composition · Non-destructive

**Supplementary Information** The online version contains supplementary material available at https://doi.org/10.1617/s11527-023-02147-3.

M. Nedeljković (✉) · P. Holthuizen · F. França de Mendonça Filho · O. Çopuroğlu · E. Schlangen
Faculty of Civil Engineering & Geosciences-Section of Materials & Environment, Delft University of Technology, Stevinweg 1, 2628 CN Delft, The Netherlands
e-mail: M.Nedeljkovic@tudelft.nl

M. Nedeljković · S. Fennis
Rijkswaterstaat, Dutch Ministry of Infrastructure and the Environment, Utrecht, The Netherlands

N. Tošić
Civil and Environmental Engineering Department, Universitat Politècnica de Catalunya, Jordi Girona 1-3, 08034 Barcelona, Spain

Published online: 15 March 2023

testing · Handheld X-ray fluorescence · Mineral resources · Sustainability

## 1 Introduction

Over the past decade, extensive research has been carried out on the utilization of recycled concrete aggregates (RCA) and the effect of their properties on the physical and mechanical properties, durability and structural behaviour of new concrete. The variations in physical and chemical properties of RCA lead to a wide range of mechanical and durability properties of mortars and concretes with RCA [1]. A primary concern for the application of RCA in concrete plants is the unknown origin of RCA: the concrete mix design needs to be modified with each new batch of RCA.

Despite extensive research activities in this field, RCA are mostly used in low-grade applications such as road construction [2]. In order to improve the quality of RCA, mixing different parent concrete waste streams should be avoided [3] and more efficient comminution technologies should be used [4]. Preselection of concrete streams requires the characterization and quality assessment of the parent concrete. Knowing the origin and the properties of parent concrete(s) can help to improve predictions of the impact of RCA on the properties of new concrete.

Over the past decades, demolition of concrete structures has principally been carried out without significant preselection and, in particular, without any preselection of concrete. Recently, a step-by-step procedure has been proposed that can be followed to characterize concrete using non-destructive test methods before its demolition [3]; assuming that no records about the parent concrete are available. The classification of concrete is based on strength and composition. The compressive strength of the parent concrete has been shown to exert a strong influence on the compressive strength of recycled aggregate concrete [3] and on the energy consumption during the crushing of concrete [5]. Visual inspection of a concrete surface can lead to direct classification of a concrete element based on characteristic signs of concrete deterioration.

Undeteriorated concrete can be the source of high-quality RCA. Characterization techniques for determining the chemical composition of RCA are needed to further enable the separation process of undeteriorated concrete structural members. A state-of-the art non-destructive technique for determining the material chemical composition, is handheld X-ray fluorescence (hXRF), owing to the compatibility with desktop XRF for cement and concrete characterization, easy installation, maintenance and large-scale applications. Furthermore, hXRF is capable of non-destructive analysis and detection of a large range of elements with no sample preparation, making it preferable for in situ testing of concrete structural members. Chemical characterization of different materials with hXRF has been presented in a comprehensive literature survey [3]. Although research has been carried out on a wide range of scientific and industrial applications of hXRF in archaeology, metals and historical mortars characterization and classification [6, 7, 8, 9, 10, 11, 12, 13, 14, 15, 16], only two studies have attempted to investigate content of chlorides and sulphates specifically on concrete surfaces using hXRF [17, 18]. No studies have investigated the concrete composition with hXRF in a systematic way. However, there are studies on a non-destructive micro-analysis technique called micro X-ray fluorescence (μXRF) for concrete element mapping.

The μXRF technique was used to obtain images of chloride profiles in concrete [19, 20, 21], to detect the presence of silane coatings in concrete [22] and to determine the content of cement paste and aggregates in concrete [23]. The technique is similar to bulk X-ray fluorescence (XRF): it contains polycapillary optics for focusing X-rays to a size of approximately 50 μm in diameter, whereas bulk XRF investigates samples with a size of approximately 10 mm in diameter [20]. Although μXRF is capable of non-destructive X-ray imaging, the instrument chamber geometry limits the sample geometry for analysis. Therefore, it cannot be applied for in situ analysis of large vertical and horizontal surfaces of concrete structures surfaces. Recent developments in the field of handheld XRF instruments allow for real time data to be collected allowing for real time measurements and decisions to be made assuming that the hXRF is used correctly [24].

Testing the composition of parent concrete before demolition can provide two types of information: (1) the composition of major components in concrete (cement and aggregates), and (2) potential minor

elements and contamination. Knowing the cement type can assist in deciding on the upcoming application for the recycled material. For example, based on the cement type in the parent concrete, one can decide whether the fine RCA would be valuable as an alternative raw material for clinker manufacturing [25–27], as a pozzolanic material [28] or as a filler [29–32]. When the goal of using RCA is $CO_2$ sequestration, the most suitable cement type in parent concrete, would be ordinary Portland cement, containing the highest CaO and calcium hydroxide ($Ca(OH)_2$) that can render them the ability to react with $CO_2$. In the context of selective demolition, research has not yet investigated the chemical composition of parent concrete before its demolition.

With this in mind, this study differentiates itself from others by the fact that it aims for pre-demolition non-destructive identification of concrete waste streams. The vast majority of studies have been focused on characterization of RCA after concrete recycling, when concrete streams have been mixed and when it is impossible to trace back the origin of the parent concrete streams. The objective of pre-demolition concrete identification is a systematic classification of the concrete structural members in order to provide groups of concrete members with similar mechanical and chemical properties. In this way, the differences in properties between recycled concrete materials and natural aggregates could be substantially reduced (in terms of composition, strength, contamination, water absorption).

For this purpose, in this research, a new method to determine the composition of concrete in an automated way was developed. The study focuses on non-destructive characterization of the chemical composition of cement and aggregates in three concrete mix designs using an hXRF analyser. Kreijger [33] showed that the skin of a concrete structure consists of three layers, the cement skin ($\sim$ 0.1 mm thick), the mortar skin ($\sim$ 5 mm) and the concrete skin ($\sim$ 30 mm). Therefore, the research hypothesis of this study is that testing the chemical composition of the surface (first concrete skin layer) will represent the cement type, whereas testing the chemical composition of the inner layers will yield the aggregate type in a relatively homogeneous environmental setting and, therefore, can be predicted from the direct element readings of hXRF. Additionally, the chemical composition of powder materials (cement and aggregates) was measured. Combined desktop XRF and energy-dispersive X-ray spectroscopy (EDS) measurements were used for validation.

## 2 Experimental program

The aim of this study was to assess the applicability of hXRF for characterizing the chemical composition of: (1) powders and (2) hardened concrete for the purpose of concrete sorting based on cement type. Therefore, the experimental program consisted of three stages, (i) testing chemical composition of different cements, supplementary cementitious materials and aggregates with hXRF, (ii) selecting the most-used cement types in order to design concrete mixtures and (iii) testing the chemical composition of the concretes.

### 2.1 Materials

Handheld X-ray fluorescence analyses of 5 cement powders (up to 90% passing 75 μm), two secondary by-products (ground granulated blast furnace slag and fly ash), limestone filler, crushed and round river sands, were performed in this study. The raw materials used in experiments, their suppliers and densities are listed in Table 1.

### 2.2 Concrete production

#### *2.2.1 Mixture design*

Three types of cement were used: CEM I 42.5 N (Portland cement), CEM II/B-V 42.5 N (Portland–fly ash cement), CEM III/B 42.5 N (GGBFS cement) (Table 2). All mixtures had an identical water-to-cement (*w/c*) ratio of 0.50 and a constant sand-to-cement and gravel-to-sand ratio. The ratios were kept constant for all mixtures in order to examine only the effect of cement type on the chemical composition of concrete surfaces.

#### *2.2.2 Mixing sequence and curing*

A 40 L mixer was used for mixing the concrete batches. The mixing procedure was as follows: gravel, river sand and cement were dry-mixed for 1 min; thereafter, water was added followed by another 2 min of mixing. No chemical admixtures were used to

**Table 1** List of raw materials

| No. | Type of the material | Supplier | Density (kg/m$^3$) |
|---|---|---|---|
| 1 | CEM I 42.5 N | ENCI Belgium | 3150 |
| 2 | CEM I 52.5 R | ENCI Belgium | 3150 |
| 3 | CEM III/A 42.5 N | ENCI Netherlands | 3015 |
| 4 | CEM III/B 42.5 N | ENCI Belgium | 3000 |
| 5 | Ground granulated blast furnace slag (GGBFS) | ECOCEM | 2900 |
| 6 | Fly ash Class V | VLIEGASUNIE | 2440 |
| 7 | Limestone filler | CALCITEC | 2650 |
| 8 | Crushed river sand (0–4 mm) | Dekker group | 2650 |
| 9 | Round river sand (0–4 mm) | Dekker group | 2650 |
| 10 | CEM II/B-V 42.5 N | BauMineral GmbH | 2910 |

**Table 2** Proportions of concrete mixtures (kg/m$^3$)

| | Concretes mixtures | | |
|---|---|---|---|
| | SC1 | SC2 | SC3 |
| CEM I 42.5 N | 370 | – | – |
| CEM II/B-V 42.5 N | – | 370 | – |
| CEM III/B 42.5 N | – | – | 370 |
| Sand 0–4 mm | 800 | 800 | 800 |
| Gravel 4–16 mm | 980 | 980 | 980 |
| Water* | 192.3 | 192.3 | 192.3 |

*Denotes water content including the aggregate absorption correction

preclude additional effects of these materials on the strength development and to enable examining only the effect of cement type on the chemical composition. After mixing, the cement concretes were cast into 150 × 150 × 150 mm$^3$ cubic moulds and compacted with a compaction table for 15 s. Subsequently, 24 h after casting, the samples were demoulded and stored in a curing chamber at a temperature of 20 °C and relative humility 99% until the age of testing. At a curing age of 90 days, the concrete samples were split into three groups to investigate the effect of surface state on chemical composition:

(1) Water saturated concrete surface: additional 10 days in the curing chamber;
(2) Air dried concrete surface: additional 10 days in open air;
(3) Oven dried concrete surface: additional 10 days in an oven at 75 °C.

## 2.3 Methods

### *2.3.1 Bulk element composition testing methods*

Supplementary Table S1 lists the methods for analysing the chemical composition of powders and hardened samples and their major features. The description of the methods is given in Sects. 2.3.1.1–2.3.1.3.

*2.3.1.1 Handheld X-ray fluorescence (hXRF) analyser* The samples were analysed using a Bruker S1 TITAN 800 handheld Energy Dispersive X-ray Fluorescence analyser (Fig. 1, left), equipped with a rhodium tube from which X-rays are emitted, and a high-resolution Silicon Drift (SDD) detector. The instrument produces an X-ray beam at a 45° angle from the centre of the analyser's tip (Fig. 1, right). Regarding filter use, it was not used for calibration method and it was shown that the signal on historical mortars, with composition similar to concrete, was the best when no filter was used [9], hence, this approach was followed in this study as well.

The hXRF spectrometer must always be in contact with sample (Fig. 1, left), not at a distance from it [35]. X-rays have a limited penetration depth of few μm to several mm, depending on the nature of the sample matrix. For that reason, the measured composition by hXRF will be representative to the outmost layers [36]. Samples were at least 10 mm thick across the beam profile to fully ensure that only the desired material was analysed, and thus, a reliable comparison between samples was obtained. The instrument was turned on at least 10 min prior to the initial measurement, to allow the detector to fully cool and reach a stable temperature. The instrument's X-ray tube was turned on

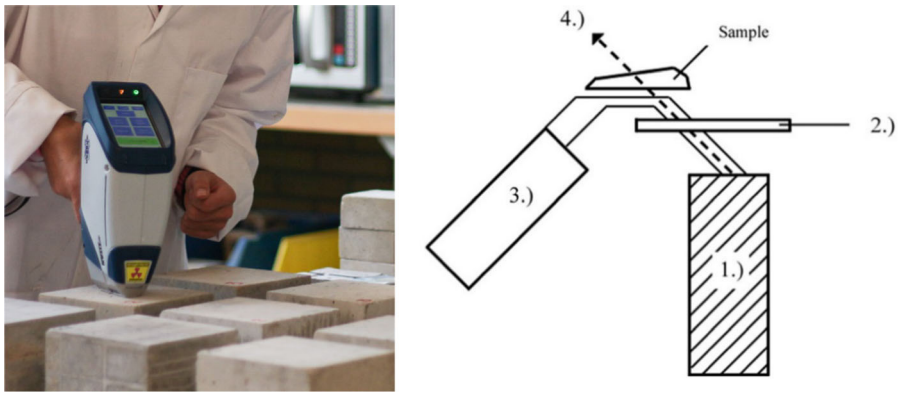


**Fig. 1** Left: instrument, right: scheme of the hXRF analyser, including: (1) X-ray source (rhodium tube); (2) filter; (3) detector; (4) beam path at 45°angle, adopted from [34]

for at least 1 min prior to the initial measurement, to help eliminate the effects of initial fluctuations in the electrical current [6]. Measurements used a 15 keV, 12.4 µA and Bruker's ARTAX$^{TM}$ SW v8 software. These settings are in accordance with calibration settings.

The calibration was performed by measuring certified reference materials including different cement types. The Bruker$^{TM}$ calibration method for cement was used, being created with samples that have a similar chemistry to the samples being analysed, therefore producing a much closer correlation with the chemical composition and enabling more accurate data to be collected in real time. Supplementary Fig. S1 shows hXRF spectra of quartz sand and limestone filler and their characteristic element peaks. The characteristic of quartz sand was the high Si concentration (95.4 wt.% ± 0.99), and that of limestone was the high Ca concentration (93.94 wt.% ± 0.15). The quartz and limestone were used to monitor for low-level contamination on the analysis range or in the detector. It should be noted that for the characterization of materials such as steel reinforcement or steel fibres in concrete, a new calibration is needed, since the calibration method for cement includes elements and their analysis ranges which are characteristic for cementitious materials (MgO, CaO, $Al_2O_3$, $SiO_2$, $P_2O_5$, $SO_3$, $K_2O$, $TiO_2$, MnO, $Fe_2O_3$).

*2.3.1.2 Desktop X-ray fluorescence (XRF) spectrometer* The chemical composition of 5 cement powders, two secondary by-products (ground granulated blast furnace slag and fly ash), limestone filler, crushed and round river sands, were also analyzed with desktop X-ray fluorescence (XRF) spectrometer. The desktop XRF measurements were performed in Heidelberg Cement Benelux laboratories in Maastricht, the Netherlands. The XRF spectra of the studied materials were recorded with a PANalytical AXIOSmAX Advanced 4 kW Rh 60 kV LiF220 Ge111-c PX1 spectrometer on pressed pellets. Regarding sample preparation for desktop XRF, loose powders were mixed with a binding agent, Boreox ($C_{12}H_{22}O_{11}$) from Fluxana. Powders were then pressed and prepared in a POLAB APM automatic sample preparation module machine with final appearance as shown in Fig. 2. The powder fineness of 80% $<$ 16 µm was required for analyses.

*2.3.1.3 Environmental scanning electron microscope and energy-dispersive X-ray Spectroscopy (ESEM-EDS)* The Thermo Scientific$^{TM}$ UltraDry EDS Detector was used for measurements. Semi-quantitative analysis was carried out with Thermo Pathfinder v1.3.22 using the standardless method. The accelerating voltage for quantitative EDS analyses is recommended to be at least 2–3 times the voltage of the element absorption edge. For example, Al, Si, Ca and Fe have the absorption edge voltage of 1.560,

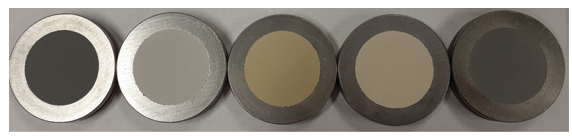

**Fig. 2** Sample preparation for desktop XRF using automatic sample preparation module machine (POLAB APM)

1.840, 4.037 and 7.110 keV respectively, implying that the accelerating voltage should be at least 8.074 (4.037 × 2) keV for Ca and 14.220 (7.110 × 2) keV for Fe, respectively [37]. Considering the main oxides expected to occur in concrete, e.g., CaO, $SiO_2$, $Al_2O_3$, $Fe_2O_3$, MgO, $SO_3$, the accelerating voltage was 15 keV to enable quantification of iron (to access K lines of iron). Previous work showed that at such a voltage, 95% of the characteristic X-rays escaping cementitious materials were generated within a depth of ~ 900–1700 nm (depending on the phase, it's density and on the measured element) [38]. The accelerating voltage of 15 keV was also used during hXRF measurements.

### 2.3.2 *Sample preparation*

*2.3.2.1 Sample preparation for powders* Regarding sample preparation for hXRF and EDS, standard powder cups covered with a foil and pressed powders were prepared [35], however, they were not providing satisfactory results for hXRF analyzed samples and the cups could also not be used for EDS analysis. Hence, a new method was proposed for testing powders, using epoxy impregnation (Fig. 3), since the epoxy can attenuate the X-rays generated for low tube voltages (< 15 keV). The samples were epoxy impregnated to also keep the particles fixed and to obtain a perfectly flat and smooth surface for hXRF contact measurements, which was not possible with the standard sample preparation method (a sample cup using 4 µm prolene or ultralene film). An additional advantage of using epoxy impregnated samples is the elimination of any air pockets which might have affected the penetration and escape of X-rays. To prepare the powder-epoxy sample, the Conpox Resin BY 158 (liquid) was mixed with the Conpox Hardener HY 2996 (Polyamine liquid) and then powder was added into it. The ratio of epoxy resin to hardener used was 3:1. The density of the epoxy resin and hardener mix was 1.16 g/cm$^3$. The mixing of epoxy resin, hardener and the powder was done through gentle stirring for 10 min to ensure dispersion of the powder and to minimize the formation of air bubbles in the sample. The mixture was then cast in a 40 mm round silicon rubber mold with a thickness of 10 mm. It was left for 24 h to harden at room temperature to ensure that the powder particles would settle on the bottom of the mould. Subsequently, the samples were ground following the procedure described in Supplementary Table S2, to obtain a very flat and smooth ("mirror-like") surface. In this study, the sample processing procedure is shown in Fig. 3. The prepared samples for element analysis are shown in Supplementary Fig. S2. It should be noted that the individual particles in powders may have different properties (e.g. size, composition, density and shape). The effect of particles properties on segregation of powder mixtures during epoxy-impregnation was not considered since powders have none or limited amount of heavy particles (e.g. particles that contain only $Fe_2O_3$). In addition, the goal of the hXRF and EDS analyses is the bulk chemical composition of powders. When powder bulk is analyzed, the aforementioned differences are averaged out and more reliable results can be obtained [39].

*2.3.2.2 Preparation of the concrete specimens* The production of concrete specimens (mix design, mixing, geometry, curing) is detailed in Sect. 2.2. Based on Kreijger's study on the concrete skin [33], determining the chemical composition of the outer surface (first concrete skin layer) would charecterize the cement type. Therefore, prior to testing, it was essential to make sure that the concrete surface is flat and free of dust or any other foreign materials. All the surfaces, except the concrete trowelled surface, were characterized using hXRF. The trowelled surface was not characterized in order to avoid localized effects such as inconsistent trowelling and trowel burn, which may affect the tip of the hXRF. The outer surfaces were cleaned with ethanol and dried with an air gun without any surface grinding, as this could have caused loss of material that is crucial for the characterization of the paste-only zone. The prepared concrete surfaces for hXRF tests are shown in Fig. 4. In order to obtain representative results on each sampling area and each concrete type, at least nine measurements were taken. The grid of nine points can be seen on the samples surfaces in Fig. 4. The grid was also used in order to evaluate the repeatability of the results, i.e. to compare the obtained results with previous measurements made at the same position. The inner layers were accessed using a diamond abrasive tool with a grit size of 60 for grinding and afterwards cleaning the concrete surface with ethanol and drying it with an air gun (Supplementary Fig. S3).

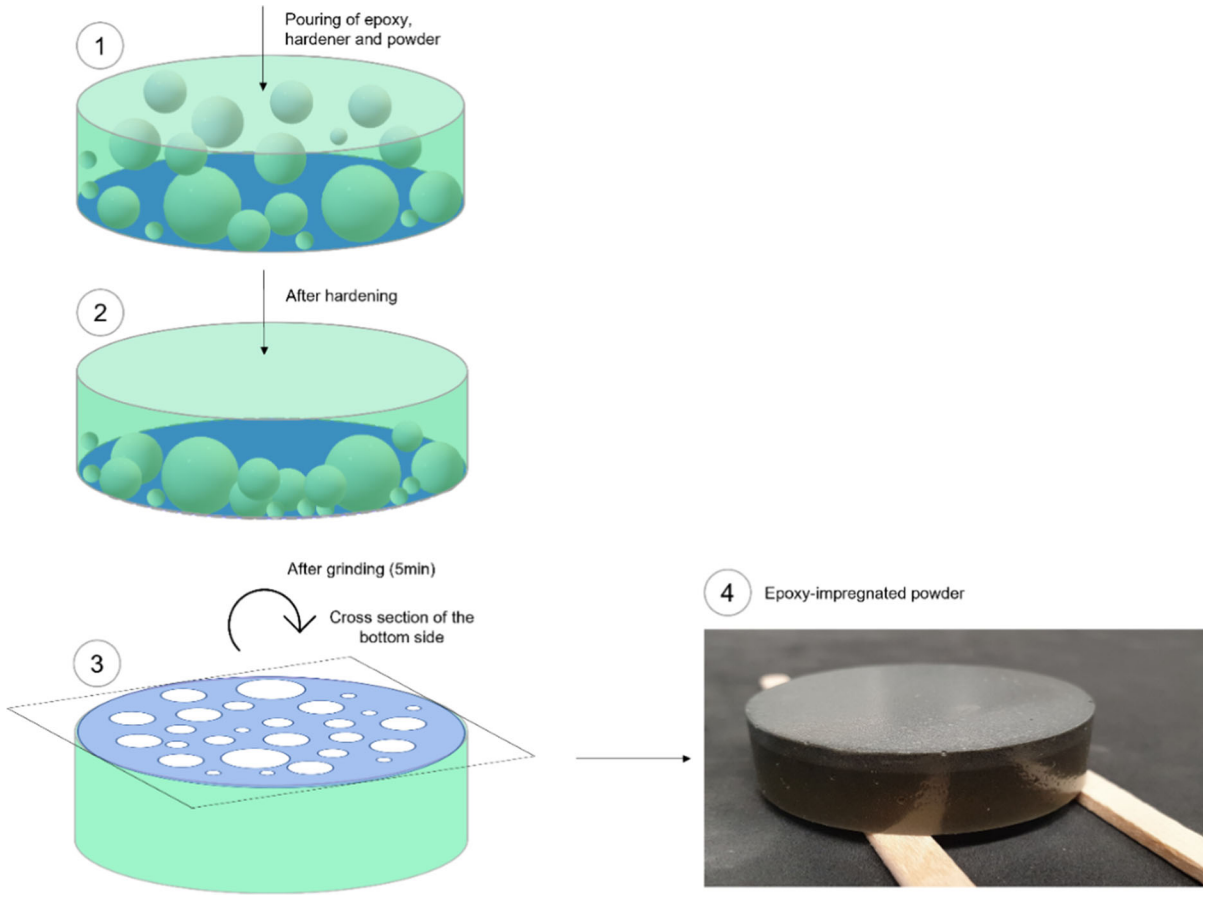


**Fig. 3** Sample preparation for hXRF and EDS using epoxy-impregnation of powders

The criteria for selecting measurement duration were based on convenience and accuracy. Usually, measurement lasts from 10 s to 10 min [40]. Shorter duration (10–30 s) is used more for qualitative scanning and sorting. Major elements in percentage concentrations can be analysed in a minute or less, whereas minor elements at part per million (PPM) concentrations may need to be analysed for 3–10 min or longer. The other and ultimately more important criterion is precision. A fluorescence spectrum in this study were recorded for 30, 60, 90 and 120 s live time on three concrete types (SC1, SC2, SC3).

Figure 5 shows the preparation and placement of a typical concrete block ($50 \times 50 \times 20\,mm^3$) inside the electron microscope for EDS surface measurements. Cutting of a concrete cube required water. Subsequently, concrete blocks were placed in an oven at 60 °C for drying until the testing. The microscope and EDS settings were kept constant for all the samples. The imaging resolution was $512 \times 384$ pixels. The image resolution was 1 μm per pixel. An example of a composite ESEM-BSE image of nine fields is presented in Fig. 5. The matrix $3 \times 3$ (00–22) was selected so that the chemical composition with a 1-μm resolution over an area larger than a single field could be determined [39].

## 3 Results and discussions

### 3.1 Bulk composition of powders with hXRF

The chemical compositions of powders obtained with hXRF are shown in Table 3. The chemical composition of the sands and limestone filler was based on a very few elements. The chemical content of sands was mainly siliceous (> 95% $SiO_2$). The limestone filler is characterized by its high CaO content. Cement

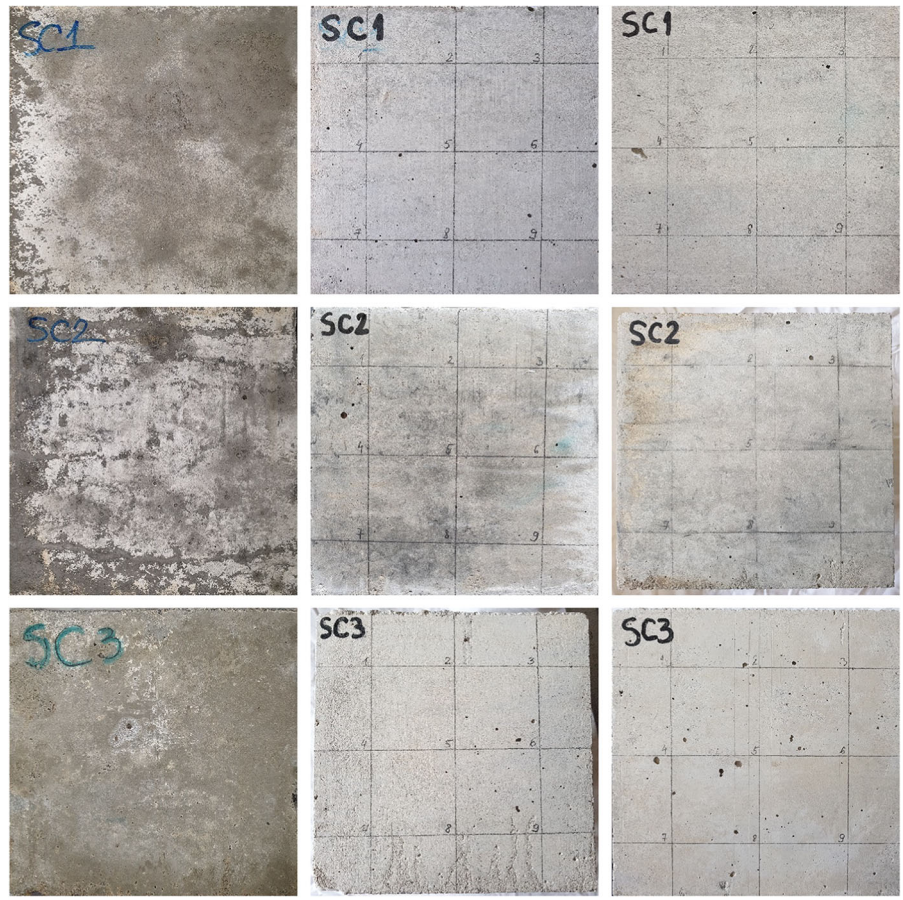


a) Water saturated b) Air-dried c) Oven-dried

**Fig. 4** Appearances of concrete surfaces (samples 150 × 150 × 150 $mm^3$) of different mixtures under three conditions: **a** water saturated, **b** air dried and **c** oven dried

powders are heterogeneous with respect to chemistry as a result of their production processes. The chemical composition of the cements can vary within wide limits, depending on the percentage of secondary by-products (fly ash and GGBFS) mixed with ordinary Portland cement. The ordinary Portland cement consists mainly of CaO and $SiO_2$, and the minor components are $Al_2O_3$, $Fe_2O_3$, MgO, $SO_3$. The CaO content of most of the cements ranged from 50 to 64%, and that of $SiO_2$ ranged from 20 to 43%. The hXRF determines precision as the margin of error or the standard deviation by analyzing X-ray counting statistics for each measurement [41]. Standard deviation can be recorded as 1σ, 2σ or 3σ. The confidence intervals are 68.27% for one standard deviation, 95.45% for two standard deviations and 99.73% for three standard deviations. The standard deviation was recorded as 3σ. Analysis showed that statistical tests revealed the expected relationship between precision and concentration of the sample where increasing concentration is followed by increasing precision (Fig. 6) as also found by Durance et al. [41]. Si, Mg and K measurement precision is more concentration dependant than of the other main elements.

## 3.2 Bulk composition of concrete samples with hXRF

### *3.2.1 Effect of concrete surface condition on hXRF measurements*

Figure 7 shows the chemical composition ($Fe_2O_3$, CaO, $SiO_2$, $Al_2O_3$, MgO, $SO_3$) of concrete surfaces in relation to their treatments (water saturated, air dried, dried). Measurement of $Fe_2O_3$ showed the best performance, its content was the same for all curing regimes. Detection of other elements was strongly dependent on the curing regime. Testing water

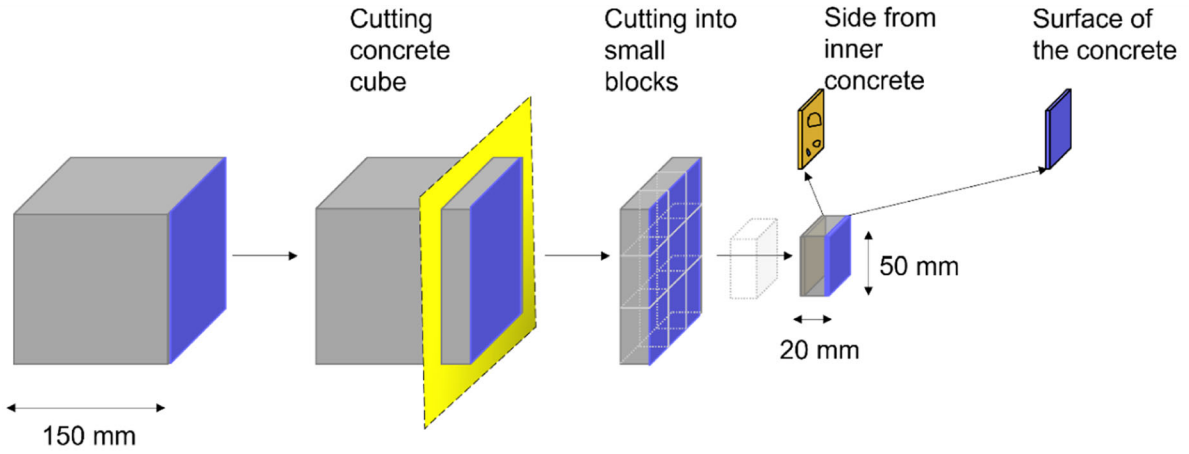
Cutting concrete cube
Cutting into small blocks
Side from inner concrete
Surface of the concrete
150 mm
50 mm
20 mm

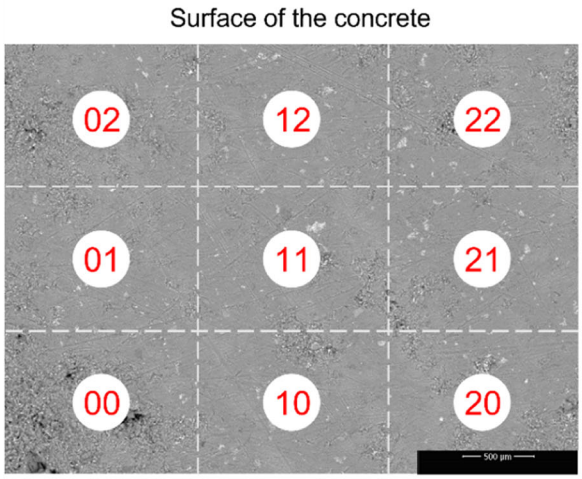
Surface of the concrete
02
12
22
01
11
21
00
10
20

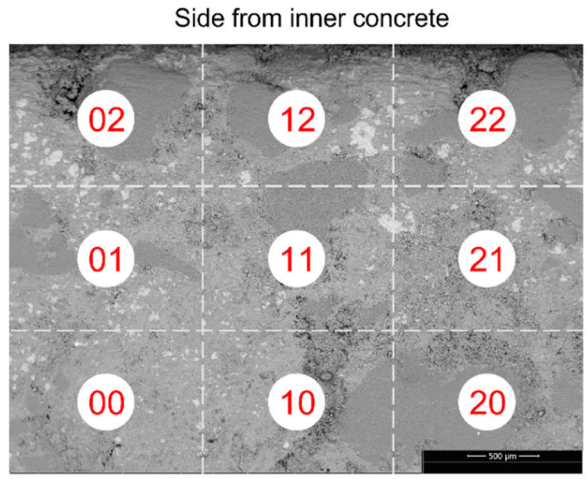
Side from inner concrete
02
12
22
01
11
21
00
10
20

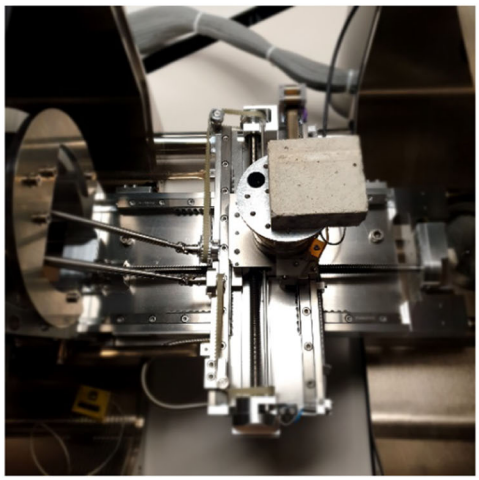


2/9/2022
8:51:14 AM
det
CCD
pressure
3.38e-4 mbar
x: -11.3953 mm
y: -6.3339 mm
z
-0.0005 mm
tilt
0 °

◀**Fig. 5** Cutting and placement of concrete block inside the electron microscope for EDS surface measurements. Blue and yellow images are the area of interests (3 × 3 matrix (fields are labelled 00–22), with an individual SI field comprising 512 × 384 pixels) for concrete surface and concrete inner characterization. All nine fields of the area were analysed under the same analytical conditions

saturated concrete surfaces resulted in a large increase in recorded concentrations for CaO, a decrease in concentrations for $SiO_2$ and $Al_2O_3$. MgO and $SO_3$ could not be identified. A high moisture content of the sample leads to the underestimation of the target element concentrations as also observed for soils [42]. The replacement of air with water in pore-spaces increases photoelectric absorption in addition to scattering since the mass attenuation coefficients are higher for water than air [43]. The photoelectric absorption is the main photon interaction process at low energies (below 100 keV) [44]. In addition, an increase in pore saturation increases the density of the sample and so increases the photoelectric absorption effect. The fluorescence from light elements will be absorbed and scattered to a greater extent in water than fluorescence from heavy elements [45] such as for example $Fe_2O_3$. Drying improves the accuracy of the results, decreasing the effect of water saturation on the recordings.

**Table 3** hXRF results for powders bulk chemical composition

| Element oxides | CEM I 42.5N (wt. %) | StdErr | CEM I 52.5R (wt. %) | StdErr | CEM II/B-V 42.5N (wt. %) | StdErr | CEM III/A 52.5N (wt. %) | StdErr | CEM III/B 42.5N (wt. %) | StdErr |
|---|---|---|---|---|---|---|---|---|---|---|
| MgO | 2.10 | 0.974 | 4.02 | 1.133 | 2.64 | 0.896 | 7.35 | 1.271 | 6.17 | 1.081 |
| $SiO_2$ | 23.83 | 0.552 | 20.01 | 0.579 | 43.35 | 0.726 | 22.74 | 0.700 | 28.75 | 0.674 |
| $Al_2O_3$ | 3.59 | 0.302 | 3.03 | 0.333 | 3.91 | 0.297 | 5.78 | 0.417 | 6.46 | 0.382 |
| $P_2O_5$ | 0.43 | 0.105 | 0.21 | 0.113 | < LLD* | | < LLD | | < LLD | |
| $SO_3$ | 1.71 | 0.051 | 2.46 | 0.064 | 1.44 | 0.053 | 3.76 | 0.082 | 4.25 | 0.078 |
| $K_2O$ | 0.38 | 0.016 | 0.35 | 0.018 | 0.56 | 0.019 | 0.43 | 0.022 | 0.44 | 0.019 |
| CaO | 63.55 | 0.122 | 64.60 | 0.134 | 41.99 | 0.105 | 55.82 | 0.133 | 50.13 | 0.116 |
| $TiO_2$ | 0.46 | 0.021 | 0.58 | 0.026 | 0.52 | 0.019 | 1.09 | 0.033 | 0.98 | 0.027 |
| $Mn_2O_3$ | 0.07 | 0.012 | 0.11 | 0.016 | 0.07 | 0.011 | 0.25 | 0.018 | 0.30 | 0.015 |
| $Fe_2O_3$ | 3.87 | 0.035 | 4.63 | 0.043 | 5.48 | 0.037 | 2.73 | 0.032 | 2.52 | 0.025 |
| Total | 100 | | 100 | | 100 | | 100 | | 100 | |

| Element oxides | GGBFS (wt. %) | StdErr | Fly ash (wt. %) | StdErr | Crushed river sand (wt. %) | StdErr | Round river sand (wt. %) | StdErr | Limestone filler (wt. %) | StdErr |
|---|---|---|---|---|---|---|---|---|---|---|
| MgO | 7.39 | 1.033 | 4.00 | 1.096 | 0.83 | 0.425 | 1.71 | 0.502 | 4.20 | 1.202 |
| $SiO_2$ | 34.93 | 0.741 | 51.15 | 1.369 | 97.73 | 0.982 | 95.45 | 0.994 | | |
| $Al_2O_3$ | 10.06 | 0.420 | 20.52 | 0.645 | 0.26 | 0.135 | 0.84 | 0.163 | 1.64 | 0.250 |
| $P_2O_5$ | < LLD | | 0.65 | 0.123 | < LLD | | < LLD | | 0.13 | 0.099 |
| $SO_3$ | 1.96 | 0.059 | 1.28 | 0.062 | < LLD | | 0.10 | 0.027 | < LLD | |
| $K_2O$ | 0.57 | 0.020 | 2.16 | 0.039 | 0.15 | 0.011 | 0.54 | 0.018 | < LLD | |
| CaO | 41.46 | 0.104 | 2.67 | 0.054 | < LLD | | 0.82 | 0.016 | 93.94 | 0.154 |
| $TiO_2$ | 1.37 | 0.027 | 1.65 | 0.025 | 0.08 | 0.006 | 0.05 | 0.007 | < LLD | |
| $Mn_2O_3$ | 0.42 | 0.015 | 0.20 | 0.012 | 0.01 | 0.004 | 0.01 | 0.005 | < LLD | |
| $Fe_2O_3$ | 1.84 | 0.016 | 15.73 | 0.056 | 0.94 | 0.009 | 0.48 | 0.008 | 0.08 | 0.023 |
| Total | 100 | | 100 | | 100 | | 100 | | 100 | |

*LLD stands for lower level detection limit

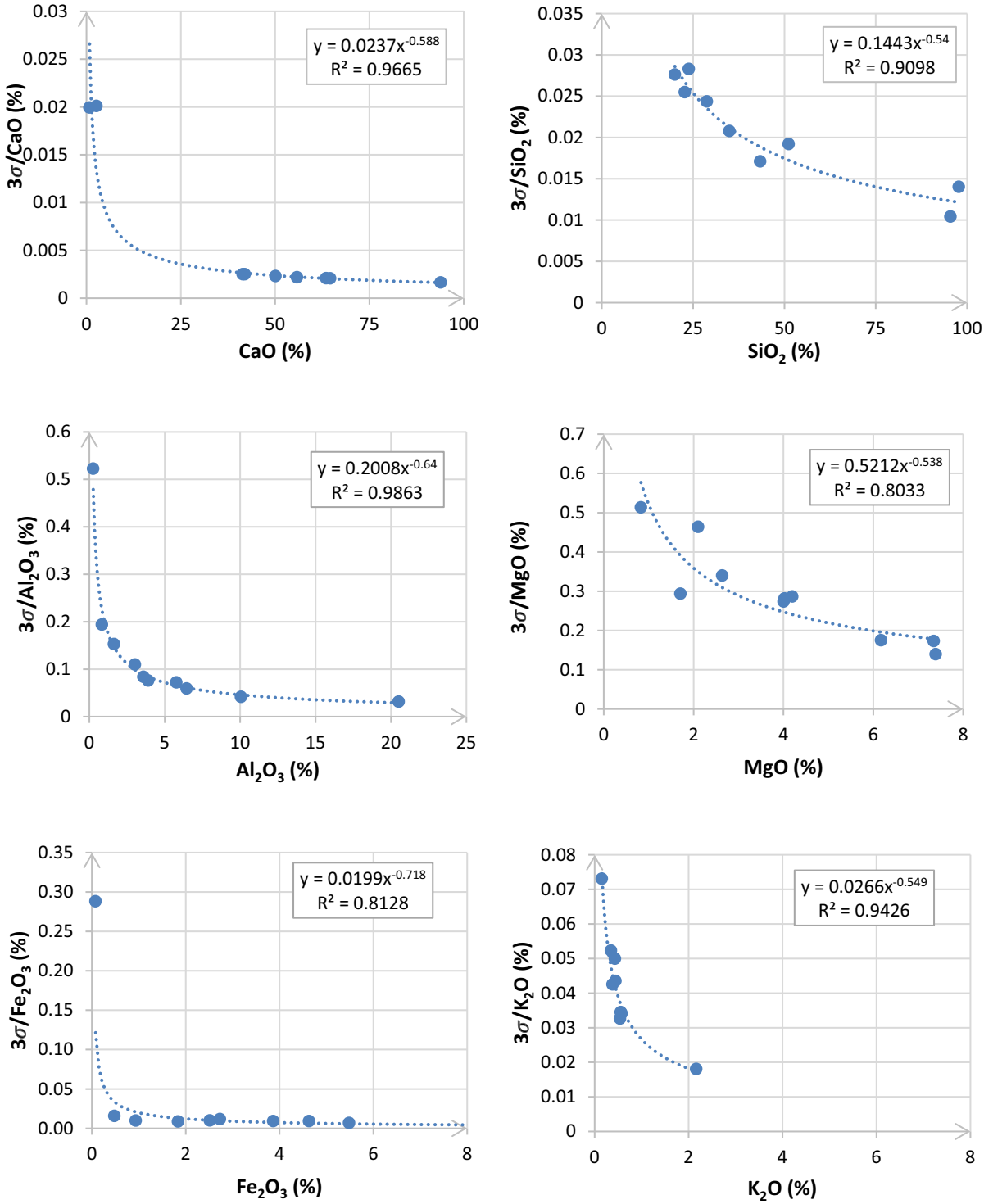


**Fig. 6** Statistical analysis for major elements (CaO and $SiO_2$) and minor elements ($Al_2O_3$, MgO, $Fe_2O_3$, $K_2O$)

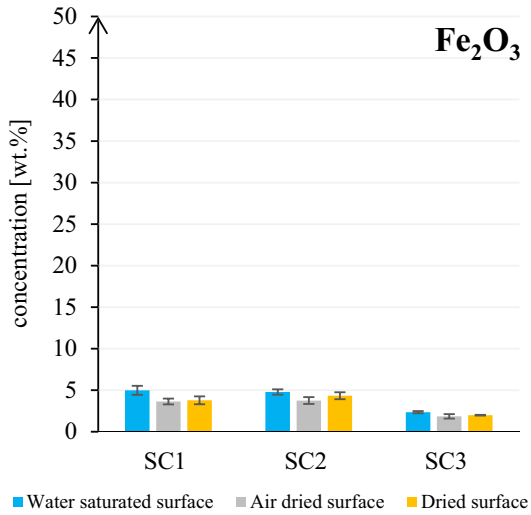
Fe2O3
concentration [wt.%]
SC1
SC2
SC3
Water saturated surface
Air dried surface
Dried surface

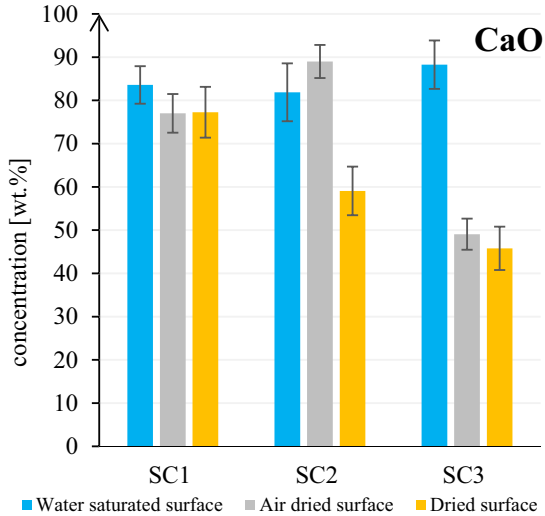
CaO
concentration [wt.%]
SC1
SC2
SC3
Water saturated surface
Air dried surface
Dried surface

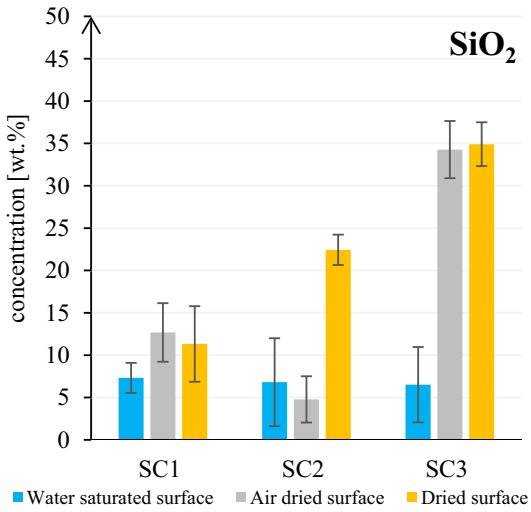
SiO2
concentration [wt.%]
SC1
SC2
SC3
Water saturated surface
Air dried surface
Dried surface

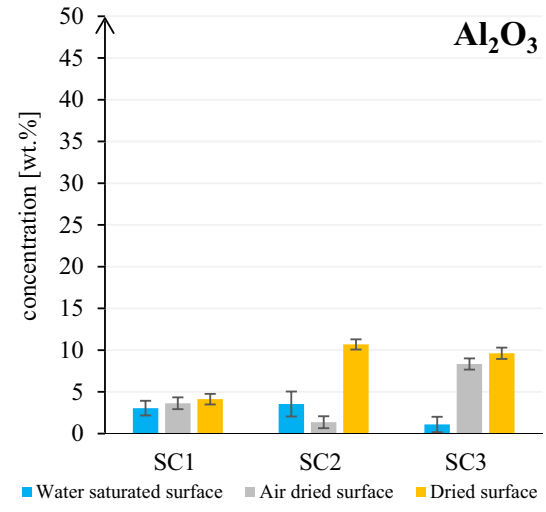
Al2O3
concentration [wt.%]
SC1
SC2
SC3
Water saturated surface
Air dried surface
Dried surface

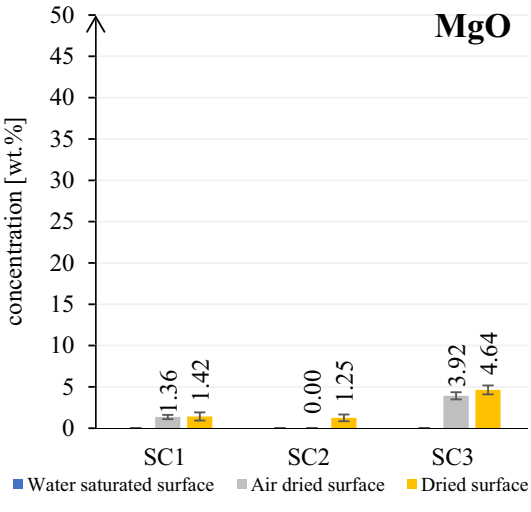
MgO
concentration [wt.%]
1.36
1.42
0.00
1.25
3.92
4.64
SC1
SC2
SC3
Water saturated surface
Air dried surface
Dried surface

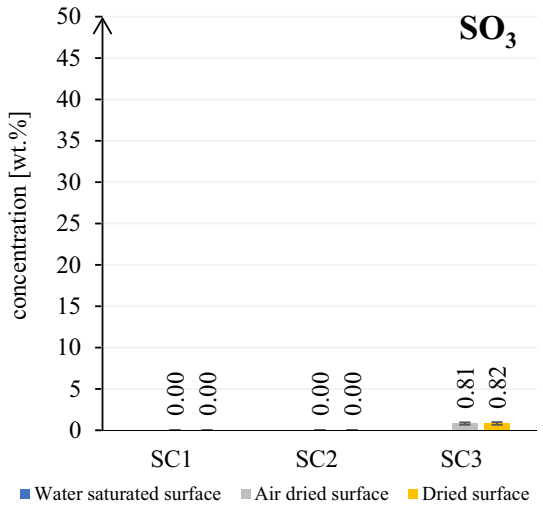
SO3
concentration [wt.%]
0.00
0.00
0.00
0.00
0.81
0.82
SC1
SC2
SC3
Water saturated surface
Air dried surface
Dried surface

◀**Fig. 7** Effect of surface state on the chemical composition of concrete surfaces

Concrete (water saturated) surfaces were enriched in CaO, which suggests Ca leaching to the surface and carbonation during curing leading to precipitation of $CaCO_3$ (white precipitates on the SC1, SC2, SC3 surfaces, Fig. 4). Carbonation is favored by $CO_2$ ions in the liquid near the concrete surface. Nevertheless, the distinction of cement types in concretes SC1 and SC2 was evident with a decrease of CaO and an increase in $SiO_2$ and $Al_2O_3$ in SC2 concrete compared with concrete SC1. Regarding the composition of SC2 and SC3 concrete surfaces, distinct concentrations can be seen among MgO, $Al_2O_3$ and $Fe_2O_3$. Although the oxide concentrations at concrete surface deviate from the original composition of powder cements, they are within the broader cement classification region [46]. These oxides (CaO, $SiO_2$, MgO, $Al_2O_3$ and $Fe_2O_3$) can be defined as characteristic oxides which can be used for concrete identification driven by cement type to facilitate fast screening of a large number of concrete elements where bulk composition of cement and aggregates is sought. For instance, cement type CEM III/B used for SC3 concrete production was recognized by the characteristic MgO concentration (which is relatively higher than that of SC1 and SC2 concretes) and a CaO:$SiO_2$ ratio of nearly 1.

### *3.2.2 Effect of measurement duration*

Figure 8 shows the effect of different measurement durations on the element concentration on the dried concrete surfaces. The surface dried state was selected for measurements based on results from Sect. 3.2.1. The chemical composition of concrete surfaces was measured for 30, 60, 90 and 120 s. The longer the measurement duration, the higher the received X-ray radiation dose. The results show that for all concretes and their elements, 30 s was sufficient and there was no significant change in element concentrations with longer measurement durations. This finding is in line with the study by Bourke and Ross [47]. Optimal beam time for routine in situ logging was c. 30 s per beam, both in mining plus mode [48] and in soil mode [47] for lithological discrimination of rock samples, ranging in composition from gabbro to rhyolite. Similarly, the study by García-Florentino et al. [15] showed that almost all the elements present in the certified reference material and historical mortars can be detected using the lowest real acquisition time (50 s), thus considering the low improvement of the level of detection increasing the real acquisition time.

### *3.2.3 Repeatability on concrete surfaces*

Table 3 shows element concentrations for SC1 dried concrete surface for three spots. The number of spots was initially nine, however, recordings were very similar (Supplementary Table S3). The goal was to evaluate the ability of hXRF to obtain consistent results when performing multiple measurements at different spots on the same sample. Each spot was scanned nine times and the average was reported. As a result, the agreement was considered acceptable for most elements among the spots, though for CaO and $SiO_2$, large standard deviations were observed. Sometimes a problem with accuracy will be indicated by a high standard deviation (counting statistics) reported by the instrument [13]. These standard deviations are considered acceptable because the instrumental standard deviation for each measurement is low, in the order of c. $\pm$ 10 wt.%. The standard deviation in Table 4 was reported as a deviation for replicate analyses which was not instrumental standard deviation. Since they were $<$ 10 wt.%, with regard to the factory reported instrumental standard deviation, these deviations were found acceptable. Furthermore, the coefficient of variation ranging from 5.5% ($Fe_2O_3$) to 33.5% ($SiO_2$) was as sensitive to the changes in the composition from one spot to other as it was the standard deviation.

### *3.2.4 Concrete's layer scanning*

When the composition data from the surface and inner layers (matrix below the surface and single aggregate with size of 16 mm) were compared for SC1 dried concrete surface, Fig. 9, it was clear that the measurements were influenced by the aggregate vol.% and composition, more than at the surface. The surface was rich in CaO compared with the inner layers, suggesting the dominant presence of cement paste at the concrete surface (as the aggregates were silicious). This confirms Kreijger's theory and our hypothesis that

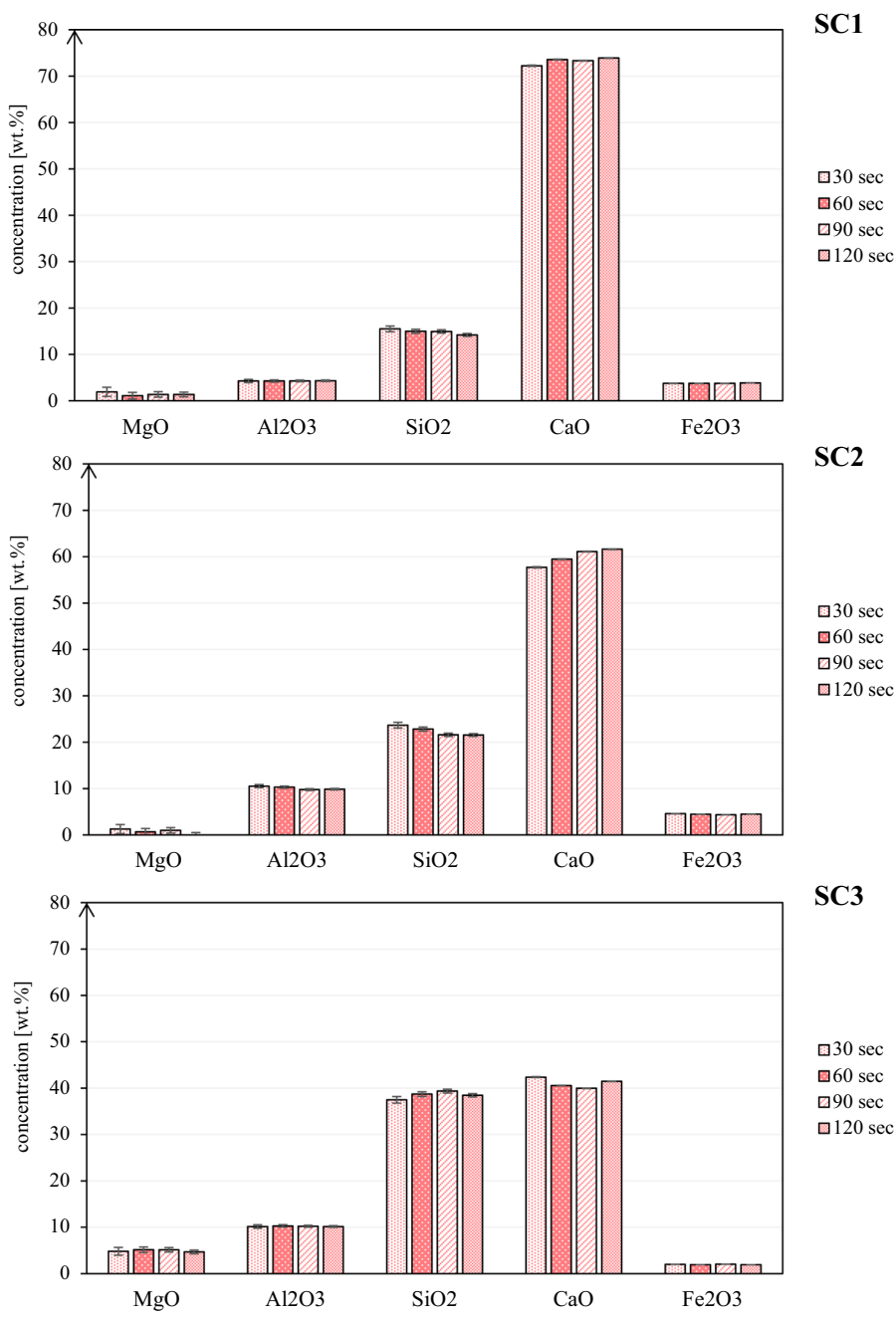


**Fig. 8** Effect of measurement duration on the chemical composition of dried concrete surfaces

the outer concrete skin is represented by the chemical composition of the cement paste [33].

Besides the chemical characterisation of the surface and inner layers, deeper inner layers have important characteristics. Variation of CaO and $SiO_2$ in inner concrete layers was due to a larger analysis spot size (5 mm X-ray beam spot size) used where it was likely to scan a mix of fine aggregates and cement paste, this effect being larger at deeper layers. Supplementary Fig. S4 shows BSE images of top concrete surfaces SC1, SC2 and SC3 (Fig. S4 a, c, e) and a close-up view of the surfaces (Fig. S4 b, d, f). Additionally, it shows the appearance of sections at 100 and 200 µm below the surface of concrete SC1 where aggregate particles

**Table 4** Repeatability of measurements for dried surface of concrete SC1

| | % | MgO | $Al_2O_3$ | $SiO_2$ | $P_2O_5$ | $K_2O$ | CaO | $TiO_2$ | MnO | $Fe_2O_3$ |
|---|---|---|---|---|---|---|---|---|---|---|
| Spot 1 | Average (wt.%) | 1.292 | 3.932 | 24.137 | 0.263 | 0.636 | 66.240 | 0.443 | 0.064 | 3.214 |
| | Std Dev (wt.%) | 0.22 | 0.68 | 8.08 | 0.09 | 0.16 | 8.56 | 0.04 | 0.01 | 0.31 |
| | CoV* (%) | 17.2 | 17.2 | 33.5 | 33.8 | 25.8 | 12.9 | 9.9 | 17.2 | 9.7 |
| Spot 2 | Average (wt.%) | 1.076 | 4.004 | 24.334 | 0.236 | 0.605 | 66.253 | 0.445 | 0.062 | 3.214 |
| | Std Dev (wt.%) | 0.13 | 0.76 | 7.14 | 0.06 | 0.15 | 7.33 | 0.04 | 0.01 | 0.21 |
| | CoV* (%) | 12.2 | 19.1 | 29.4 | 27.1 | 24.1 | 11.1 | 8.1 | 9.7 | 6.4 |
| Spot 3 | Average (wt.%) | 1.122 | 3.986 | 23.216 | 0.245 | 0.650 | 67.064 | 0.456 | 0.064 | 3.267 |
| | Std Dev (wt.%) | 0.14 | 0.59 | 5.43 | 0.06 | 0.17 | 5.85 | 0.03 | 0.01 | 0.18 |
| | CoV* (%) | 12.3 | 14.8 | 23.4 | 25.3 | 26.2 | 8.7 | 7.2 | 14.1 | 5.5 |

*Coefficient of variation

become more dominant (Fig. S4 g, h). Compared with the surface layer, a doubled content of $SiO_2$ was already measured at 100 µm below the concrete surface. Further study in this region (0–100 µm) is required to identify the exact depth at which the composition of aggregates has a critical influence on the measurements by taking different particle size distributions (e.g. 0/8 mm, 0/16 mm, 0/32 mm) and wall effects (related to w/c ratio) into account.

### 3.3 Powder chemical composition: hXRF versus desktop XRF results

In this study non-destructive handheld XRF data were compared to data obtained by commonly used laboratory techniques as a way of evaluating the ability of the non-destructive technique to discriminate among different powdered materials and hardened concretes.

The element concentration obtained by hXRF for powders was compared to data obtained by desktop XRF and EDS measurement techniques under laboratory conditions (Supplementary Table S4, Supplementary Fig. S5). Comparable concentration values within ± 5% were observed for all elements, particularly in the case of sand, limestone powder and CEM I. The results for the other powder materials are shown in Supplementary Tables S5, S6, S7. The results from hXRF and desktop XRF are presented side by side combined in Fig. 10 for CaO wt.% and $SiO_2$ wt.% to illustrate the accuracy for high elements concentrations. A comparison of the data showed the variation expressed as a standard error of the two techniques to be similar. This is expected since powders pass procedures such as drying, crushing, grinding, sieving and homogenising such that the composition analysis is fully comparable among different analytical techniques. Previous studies of Chinchón-Payá et al. [17, 18] evaluating chlorides content on concrete surfaces using hXRF also observed consistent results between hXRF and standardised analytical acid-soluble titration method. Similarly, Hunt and Speakman [7] showed that the hXRF clay/sediment calibration calculates highly accurate concentrations for the mid-Z trace elements performing almost identical to the desktop XRF.

### 3.4 Concrete chemical composition: hXRF versus EDS results

Compared to materials of natural origin such as soils, rocks, clays, sediments, whose composition is strongly dependent on the result of the erosion of the earth's crust over a vast timespan [49], concrete production has always been man-controlled under standard specifications such as given by EN 206: 2013 [50]. In such standards, concrete ingredients need to satisfy the requirements given by the product norms for cement [46] and aggregates [51]. An example of such requirements is the composition of these ingredients, which must be certified in order to be used in concrete. This makes concrete chemical characterization relatively less complex compared with natural materials, considering large geochemical variations in natural materials. However, as the original project documents

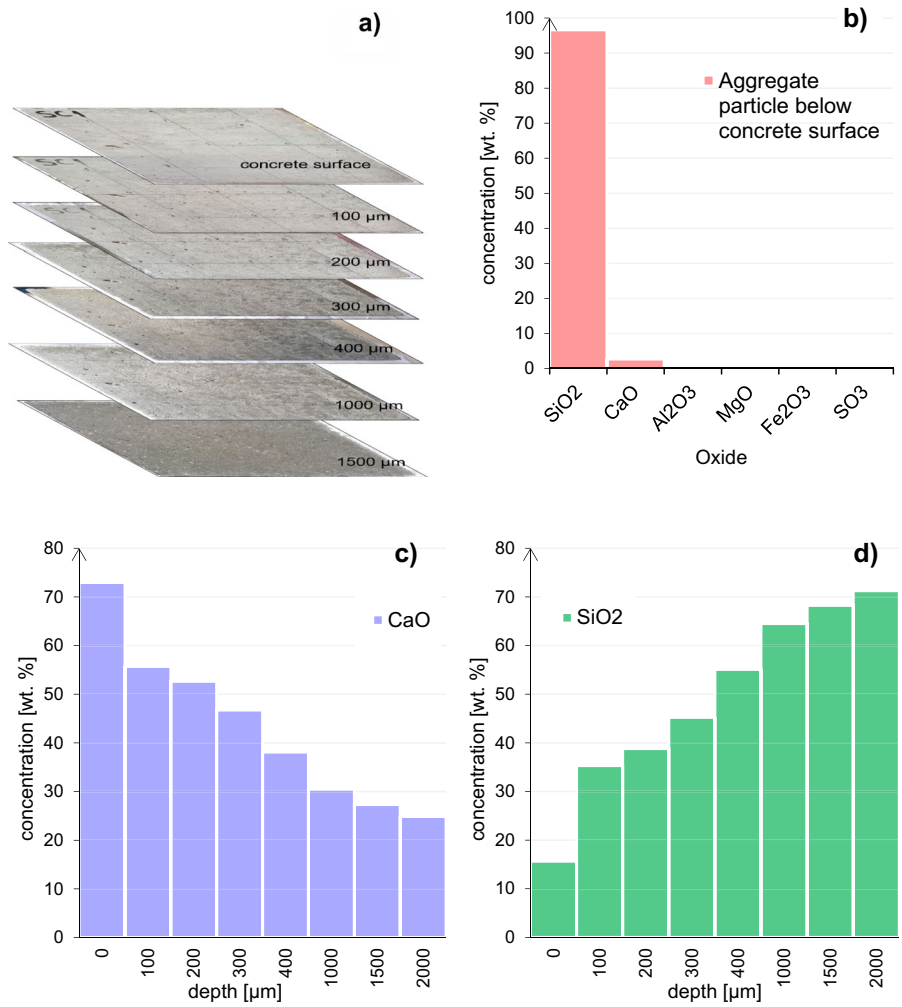


**Fig. 9** **a** Layer by layer measurement scheme, **b** composition of a single aggregate (D = 16 mm) in one of the inner layers, **c** CaO and **d** $SiO_2$ content as a function of depth in dried concrete sample SC1, (1st) depth: 0 µm, (2nd) depth: 100 µm, (3rd) depth: 200 µm, (4th) depth: 300 µm, (5th) depth: 400 µm, (6th) depth: 1000 µm, (7th) depth: 1500 µm, (8th) depth: 2000 µm

of the aged concrete structures are often not available, applying forensic materials engineering protocols for concrete characterization is essential.

Non-destructive chemical composition characterization of concrete using hXRF was evaluated in this study since it can be performed in situ, unlike other destructive methods which have been employed to characterize and control the chemical compositions of cement materials and products in the laboratory conditions (desktop XRF, EDS, electron probe microanalysis, inductively coupled plasma optical emission spectrometer). The hXRF technique may speed up parent concrete identification in a structure prior to its demolition, and make it possible to classify concrete elements with different chemical composition or potential contamination.

Based on EN 197-1:2011 [46], the cement classes contain 34 clinker systems, 27 products in the family of common cements and 7 products in the family of sulfate resisting common cements. These cement classes are defined based on the content of the main constituents: clinker, blast furnace slag, silica fume, pozzolana, fly ash, burnt shale and limestone. These constituents (when present in a concrete mix as a blended cement) cannot be individually identified with hXRF. Nevertheless, the bulk cement chemical

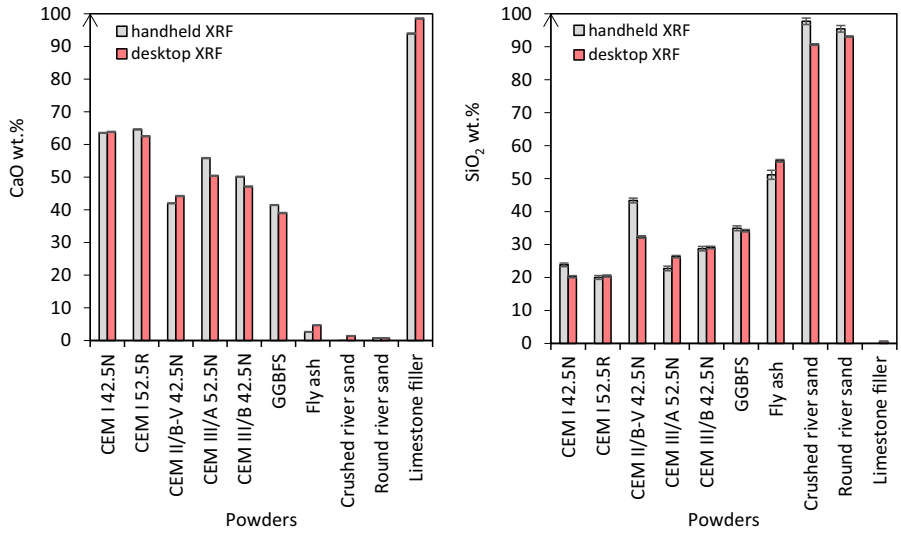


**Fig. 10** Element concentrations obtained with hXRF and desktop XRF for powders. Error bars for variation are also potted

**Table 5** Chemical composition of the concrete surfaces

| | Method | Gravel | | Concrete surface SC1 | | Concrete surface SC2 | | Concrete surface SC3 | |
|---|---|---|---|---|---|---|---|---|---|
| | | wt.% | StdErr | wt.% | StdErr | wt.% | StdErr | wt.% | StdErr |
| CaO | hXRF | 0.81 | ± 0.02 | 72.25 | ± 0.14 | 59.07 | ± 0.15 | 45.79 | ± 2.02 |
| | EDS | 0.92 | ± 0.09 | 63.86 | ± 0.13 | 44.21 | ± 0.14 | 47.11 | ± 0.14 |
| $SiO_2$ | hXRF | 91.81 | ± 0.99 | 15.5 | ± 0.26 | 22.43 | ± 0.30 | 34.91 | ± 1.94 |
| | EDS | 95.85 | ± 0.04 | 20.23 | ± 0.33 | 32.28 | ± 0.38 | 29.11 | ± 0.37 |
| $Al_2O_3$ | hXRF | 0.84 | ± 0.16 | 4.26 | ± 0.24 | 10.68 | ± 0.27 | 9.62 | ± 0.54 |
| | EDS | 1.7 | ± 0.19 | 4.84 | ± 0.13 | 10.90 | ± 0.18 | 10.02 | ± 0.18 |
| MgO | hXRF | 1.70 | ± 0.01 | 1.92 | ± 1.05 | 1.25 | ± 1.03 | 4.64 | ± 0.52 |
| | EDS | 1.65 | ± 0.07 | 1.65 | ± 0.07 | 1.21 | ± 0.06 | 5.89 | ± 0.14 |
| $Fe_2O_3$ | hXRF | 0.48 | ± 0.01 | 3.75 | ± 0.04 | 4.33 | ± 0.04 | 1.99 | ± 0.05 |
| | EDS | 0.60 | ± 0.02 | 3.28 | ± 0.05 | 3.81 | ± 0.06 | 1.19 | ± 0.03 |
| $SO_3$ | hXRF | – | – | – | – | – | – | 0.82 | ± 0.21 |
| | EDS | – | – | 0.29 | ± 0.03 | 0.57 | ± 0.03 | 2.82 | ± 0.07 |

composition can be analysed with hXRF and typical ranges for oxides can be defined using the minimum and maximum values for cement types' compositions as shown in Supplementary Table S8. Table 5 gives an overview of hXRF and EDS results for chemical compositions of concrete surfaces SC1, SC2 and SC3. Concrete classification is based on cement key characteristic oxides in chemical composition measured by hXRF and subdivided into: high, medium, and low CaO, $SiO_2$, $Al_2O_3$, $Fe_2O_3$, MgO and their ratios, as demonstrated in Supplementary Fig. S6. It is certainly needed to have at least two or more characteristic elements to identify the cement type. This means that for any cement type, a representative characteristic group of oxides can be found. For example, CEM I includes high CaO, low $SiO_2$, $Al_2O_3$, MgO, CEM II B/V is composed of medium CaO, $SiO_2$, $Al_2O_3$, low MgO, CEM III/B has characteristic high MgO, medium CaO, $SiO_2$, $Al_2O_3$, low $Fe_2O_3$. Subsequently, concretes with cement types CEM I (SC1), CEM II B/V (SC2) and CEM III/B (SC3) can be separated.

This classification broadly supports the work of other studies on the identification of different materials based on their major element oxides. Since there are still no studies on systematic concrete composition analysis with hXRF available in the literature, examples of rocks close to concrete origin are used. Such an example is limestone, the main source of CaO to make clinker for cement manufacturing [52]. Different limestones (calcarenite, sandy or bioclastic limestones) were distinguished based on their element concentrations such as of Ca, K, Rb, Sr, Ti and Zr measured with hXRF [53]. The in situ use of hXRF allowed for the identification of Normandy Chalkstone sources (dedolomitized, quartz-glauconite, calcarenite, bryozoan and grainy chalkstone) preserved in archaeological sites based on concentrations of CaO, $SiO_2$ and Sr [54]. The hXRF has been used for quality control and suitability of quartz for an industrial lot at a ferrosilicon plant [55, 56]. Critical elements (contaminants) such as iron, titanium and aluminum were analysed with hXRF in situ on a block of quartz (10-cm-side) with an accuracy of 13% for $Fe_2O_3$, $TiO_2$ and CaO (accuracy for $Al_2O_3$ was 24%) [55]. Classification of obsidian sources from volcanic glasses, rocks, artificial glasses or slags was also done based on the major element composition with hXRF [57].

Note that concrete characterization is generally more challenging compared with powder analysis. This is because powders are usually dried and homogeneous whereas the concrete specimens are much more heterogeneous (causing more sampling uncertainty). Concrete contains random assemblage of phases of different compositions and of varying shapes and sizes. Furthermore, concrete contains free and structural water attracting $CO_2$ as shown in Sect. 3.2.1 unlike powders. Preparation of samples may also introduce water. For example, the comparison of hXRF and EDS data (Table 5) has shown that the concentrations of elements measured with hXRF are not always in line with those measured with EDS. It shows also that the results of hXRF were not systematically higher or lower. The discrepancy between hXRF and EDS measurements of the concrete surface can be attributed to several reasons. To prepare a concrete surface for EDS analysis it is necessary to cut a block that can fit EDS stage (Fig. 5). Cutting requires wetting. This step might attract $CO_2$ and further precipitation of carbonates on the concrete surface. Drying concrete surface eliminates matrix issues related to water; however, structural water and carbonates ($CaCO_3$) may remain. Fine grinding of the concrete surface with ultrafine sandpaper (P-grade 2000) of grit size smaller than 10 μm can be done for improved sample preparation (e.g. removing surface $CaCO_3$). Use of coarser sandpaper may lead to the characterization of the cement mortar rather than the cement paste since a double content of $SiO_2$ is measured at 100 μm below the concrete surface (Fig. 9). The two techniques, hXRF and EDS, have also different settings such as, more controlled working conditions during EDS analysis (vacuum vs air). Moreover, having used the standardless method instead of standards-based microanalysis could lead to a large difference especially for the elements having low concentrations [58]. Further experiments, using a broader range of cements, would help to establish a greater degree of accuracy on this matter.

Regarding concrete sampling uncertainty in the laboratory conditions, in order to produce accurate element concentrations, hXRF analysis has been performed on flat concrete surfaces and multiple measurements were done at different spots on the same sample (Sect. 3.2.3) to obtain good quality estimates similarly to rocks bulk analysis [59, 60]. Considering the concrete surface preparation of existing concrete structures exposed for years under different environmental conditions in the field, a proper cleaning of the surface (free from dust, salts, loose material, surface coatings, membranes, repair products, injection materials) and surface preparation without removal of concrete skin (cement paste) are key tasks for future studies.

## 4 Conclusions

In this experimental study, non-destructive characterization of cementitious powders and concrete compositions using handheld XRF was performed. The effect of concrete surface condition (water-saturated, air-dried and oven-dried), measurement duration (30, 60, 90, 120 s), repeatability on concrete surface and concrete's layer scanning were studied. The following conclusions were drawn:

(1) Selected powders were tested using hXRF and BRUKER calibration method for cement. The cross validation of hXRF results was performed

with results from desktop XRF and EDS for two main element oxides $SiO_2$ and CaO. It was found that a linear model fits both experimental data well, with a coefficient of determination ($R^2$) of 0.995 for the hXRF-desktop XRF results and 0.991 for the hXRF-EDS results.

(2) The recognition of cement type can be challenging due to similar chemical compositions such as between CEM II/B-V and CEM III/B. A cement type can be defined by introducing characteristic element oxides and typical ranges for oxides. The oxide ranges can be defined using the minimum and maximum values for cement components as defined in EN 197–1:2011.

(3) Identification of the main elements on the concrete surface (CaO, $SiO_2$, $Al_2O_3$, $Fe_2O_3$, MgO) with hXRF using BRUKER calibration method for cement was performed in a relatively short time (minimum 30 s). The hXRF technique shows an accuracy at a level of 5% or less for the determination of high element concentrations.

(4) The curing of concrete affects the results. The water-saturated state shows that the CaO content is overestimated, specifically for concrete SC1 with CEM I (Portland cement). The Ca leaching to the concrete surface and subsequent carbonation are the main reason for this behaviour. This behavior is less obvious in concrete specimens SC2 and SC3 because of their lower CaO content compared with concrete SC1. Drying of surfaces prior to hXRF testing is shown to be more appropriate for chemical composition measurements.

(5) CEM III/B (GGBFS cement) used for SC3 concrete production is recognized by a characteristic MgO concentration (which is higher than for SC1 and SC2 concretes).

(6) A clear distinction can be made between concrete surface (represented by cement paste) and inner layers (represented by the cement mortar and aggregates) using $SiO_2$ and CaO as characteristic element oxides. There is a clear difference with regard to the high content of $SiO_2$ at the inner sections compared with the surface, confirming the siliceous composition of the aggregates used for production of concretes.

(7) Testing the composition of concrete surfaces using calibration method for cementitious powders is shown to be feasible. Although results for repeatability showed high precision, development of calibration method for typical concrete compositions and surface preparation protocols will improve the concrete surface measurements.

Finally, it can be concluded that the hXRF shows considerable potential as a non-destructive technique with minimal sample preparation for rapidly assessing chemical composition and quality of concrete. This would be helpful for ensuring identification of concrete at the source, improving the demolition efficiency and guiding the quality of recycled concrete. A follow-up study is designed to identify exact depth at which the composition of aggregates has a critical influence on the measurements taking into account different aggregate content, particle size distributions (e.g. 0/8 mm, 0/16 mm, 0/32 mm) and the wall effects (*w/c* ratio), as this is the case in practice for existing structures.

**Acknowledgements** The first author acknowledges the funding provided by the Ministry of Infrastructure and Water Management of the Netherlands (Rijkswaterstaat), SKKB and in-kind contributions from Scientific Benelux and Proceq. Special thanks to Arjan Thijssen and Maiko van Leeuwen for assistance with laboratory testing and concrete casting. ENCI-lab Maastricht is acknowledged for their valuable help on powder characterization with desktop XRF.

**Declarations**

**Conflict of interest** The authors have no competing interests to declare that are relevant to the content of this article.

## References


1. Nedeljković M, Visser J, Šavija B, Valcke S, Schlangen E (2021) Use of fine recycled concrete aggregates in concrete: a critical review. J Build Eng 38:102196. https://doi.org/10.1016/j.jobe.2021.102196
2. Zhang C, Hu M, Yang X, Miranda-Xicotencatl B, Sprecher B, Di Maio F, Zhong X, Tukker A (2020) Upgrading construction and demolition waste management from downcycling to recycling in the Netherlands. J Cleaner Prod 266:121718. https://doi.org/10.1016/j.jclepro.2020.121718
3. Nedeljković M, Tošić N, Schlangen E, Fennis S (2022) Predemolition concrete waste stream identification: Classification framework. Under review
4. Lotfi S (2016) C2CA Concrete recycling process, PhD thesis, Delft University of Technology, The Netherlands. https://doi.org/10.4233/uuid:70505a1f-c0d7-47c7-ab62-8d487761c021
5. Nedeljković M, Kamat A, Holthuizen P, Tošić N, Schlangen E, Fennis S (2022) Energy consumption of a laboratory jaw crusher during normal and high strength concrete recycling. Under review
6. Johnson J (2014) Accurate measurements of low Z elements in sediments and archaeological ceramics using portable X-ray fluorescence (PXRF). J Archaeol Method Theory 21(3):563–588. https://doi.org/10.1007/s10816-012-9162-3
7. Hunt AM, Speakman RJ (2015) Portable XRF analysis of archaeological sediments and ceramics. J Archaeol Sci 53:626–638. https://doi.org/10.1016/j.jas.2014.11.031
8. Karydas AG (2007) Application of a portable XRF spectrometer for the non-invasive analysis of museum metal artefacts. Annali di Chimica: J Anal Environ Cult Herit Chem 97(7):419–432. https://doi.org/10.1002/adic.200790028
9. Mendonça Filho FF, Morillas H, Derluyn H, Maguregui M, Grégoire D (2019) In-situ versus laboratory characterization of historical site in marine environment using X-ray fluorescence and Raman spectroscopy. Microchem J 147:905–913. https://doi.org/10.1016/j.microc.2019.02.014
10. Gallhofer D, Lottermoser BG (2018) The influence of spectral interferences on critical element determination with portable X-ray fluorescence (pXRF). Minerals 8(8):320. https://doi.org/10.3390/min8080320
11. Gallhofer D, Lottermoser BG (2020) The application of pXRF for the chemical and mineralogical characterization of heavy mineral sands. Geochem Explor Environ Anal 20(1):99–111. https://doi.org/10.1144/geochem2019-015
12. Quiniou T, Laperche V (2014) An assessment of field-portable X-ray fluorescence analysis for nickel and iron in laterite ore (New Caledonia). Geochem Explor Environ Anal 14(3):245–255. https://doi.org/10.1144/geochem2012-159
13. Hall GE, Bonham-Carter GF, Buchar A (2014) Evaluation of portable X-ray fluorescence (pXRF) in exploration and mining: phase 1, control reference materials. Geochem Explor Environ Anal 14(2):99–123. https://doi.org/10.1144/geochem2013-241
14. Calparsoro E, Maguregui M, Morillas H, Arana G, Iñañez JG (2019) Non-destructive screening methodology based on ED-XRF for the classification of medieval and post-medieval archaeological ceramics. Ceram Int 45(8):10672–10683. https://doi.org/10.1016/j.ceramint.2019.02.138
15. García-Florentino C, Maguregui M, Morillas H, Marcaida I, Madariaga JM (2017) A fast in situ non-invasive approach to classify mortars from a construction of high historical value. Microchem J 133:104–113. https://doi.org/10.1016/j.microc.2017.03.020
16. Bloise A, Miriello D (2022) Distinguishing asbestos cement from fiber-reinforced cement through portable μ-Raman spectroscopy and portable X-ray fluorescence. Environ Monit Assess 194(10):679. https://doi.org/10.1007/s10661-022-10343-x
17. Chinchón-Payá S, Torres Martín JE, Silva Toledo A, Sánchez Montero J (2021) Quantification of chlorides and sulphates on concrete surfaces using portable X-ray fluorescence. Optimization of the measurement method using monte carlo simulation. Materials 14(24):7892. https://doi.org/10.3390/ma14247892
18. Chinchón-Payá S, Torres Martín JE, Rebolledo Ramos N, Sánchez Montero J (2021) Use of a handheld x-ray fluorescence analyser to quantify chloride ions in situ: a case study of structural repair. Materials 14(3):571. https://doi.org/10.3390/ma14030571
19. Davis JM, Newbury DE, Fahey A, Ritchie NW, Vicenzi E, Bentz D (2011) Bridging the micro-to-macro gap: a new application for micro X-ray fluorescence. Microsc Microanal 17(3):410–417. https://doi.org/10.1017/S1431927611000183
20. Moradllo MK, Sudbrink B, Hu Q, Aboustait M, Tabb B, Ley MT, Davis JM (2017) Using micro X-ray fluorescence to image chloride profiles in concrete. Cem Concr Res 92:128–141. https://doi.org/10.1016/j.cemconres.2016.11.014
21. Peterson K, Julio-Betancourt G, Sutter L, Hooton RD, Johnston D (2013) Observations of chloride ingress and calcium oxychloride formation in laboratory concrete and mortar at 5 C. Cem Concr Res 45:79–90. https://doi.org/10.1016/j.cemconres.2013.01.001
22. Sudbrink B, Moradllo MK, Hu Q, Ley MT, Davis JM, Materer N, Apblett A (2017) Imaging the presence of silane coatings in concrete with micro X-ray fluorescence. Cem Concr Res 92:121–127. https://doi.org/10.1016/j.cemconres.2016.11.019
23. Yio MHN, Ho YW, Abdul Wahid F, Wong HS, Buenfeld NR (2022) Analysis of cement paste and aggregate content of concrete using micro X-ray fluorescence. Mag Concr Res 74(17):889–904. https://doi.org/10.1680/jmacr.21.00094
24. Brand NW, Brand CJ (2014) Performance comparison of portable XRF instruments. Geochem Explor Environ Anal 14(2):125–138. https://doi.org/10.1144/geochem2012-172
25. Schoon J, De Buysser K, Van Driessche I, De Belie N (2015) Fines extracted from recycled concrete as alternative raw material for Portland cement clinker production. Cem Concr Compos 58:70–80. https://doi.org/10.1016/j.cemconcomp.2015.01.003
26. Kwon E, Ahn J, Cho B, Park D (2015) A study on development of recycled cement made from waste cementitious powder. Constr Build Mater 83:174–180. https://doi.org/10.1016/j.conbuildmat.2015.02.086

27. Bordy A, Younsi A, Aggoun S, Fiorio B (2017) Cement substitution by a recycled cement paste fine: role of the residual anhydrous clinker. Constr Build Mater 132:1–8. https://doi.org/10.1016/j.conbuildmat.2016.11.080
28. Kalinowska-Wichrowska K, Kosior-Kazberuk M, Pawluczuk E (2019) The properties of composites with recycled cement mortar used as a supplementary cementitious material. Materials 13(1):64. https://doi.org/10.3390/ma13010064
29. Angulo SC, Ulsen C, John VM, Kahn H, Cincotto MA (2009) Chemical–mineralogical characterization of C&D waste recycled aggregates from São Paulo. Brazil Waste Manage 29(2):721–730. https://doi.org/10.1016/j.wasman.2008.07.009
30. Florea MVA, Ning Z, Brouwers HJH (2014) Activation of liberated concrete fines and their application in mortars. Constr Build Mater 50:1–12. https://doi.org/10.1016/j.conbuildmat.2013.09.012
31. Braga M, de Brito J, Veiga R (2014) Reduction of the cement content in mortars made with fine concrete aggregates. Mater Struct 47(1):171–182. https://doi.org/10.1617/s11527-013-0053-1
32. Oksri-Nelfia L, Mahieux PY, Amiri O, Turcry P, Lux J (2016) Reuse of recycled crushed concrete fines as mineral addition in cementitious materials. Mater Struct 49(8):3239–3251. https://doi.org/10.1617/s11527-015-0716-1
33. Kreijger PC (1984) The skin of concrete composition and properties. Mat Constr 17(4):275–283. https://doi.org/10.1007/BF02479083
34. Nazaroff AJ, Prufer KM, Drake BL (2010) Assessing the applicability of portable X-ray fluorescence spectrometry for obsidian provenance research in the Maya lowlands. J Archaeol Sci 37(4):885–895. https://doi.org/10.1016/j.jas.2009.11.019
35. Laperche V, Lemière B (2020) Possible pitfalls in the analysis of minerals and loose materials by portable xrf, and how to overcome them. Minerals 11(1):33. https://doi.org/10.3390/min11010033
36. Maróti B, Polonkai B, Szilágyi V, Kis Z, Kasztovszky Z, Szentmiklósi L, Székely B (2020) Joint application of structured-light optical scanning, neutron tomography and position-sensitive prompt gamma activation analysis for the non-destructive structural and compositional characterization of fossil echinoids. NDT E Int 115:102295. https://doi.org/10.1016/j.ndteint.2020.102295
37. Wang S, Baxter L, Fonseca F (2008) Biomass fly ash in concrete: SEM EDX and ESEM analysis. Fuel 87(3):372–379. https://doi.org/10.1016/j.fuel.2007.05.024
38. Wilson W, Sorelli L, Tagnit-Hamou A (2018) Automated coupling of nanoindentation and quantitative energy-dispersive spectroscopy (NI-QEDS): a comprehensive method to disclose the micro-chemo-mechanical properties of cement pastes. Cem Concr Res 103:49–65. https://doi.org/10.1016/j.cemconres.2017.08.016
39. Nedeljković M, Ghiassi B, Ye G (2021) Role of curing conditions and precursor on the microstructure and phase chemistry of alkali-activated fly ash and slag pastes. Materials 14(8):1918. https://doi.org/10.3390/ma14081918
40. Shackley MS (2010) X-ray fluorescence spectrometry (XRF) in geoarchaeology. Springer. https://doi.org/10.1007/978-1-4419-6886-9
41. Durance P, Jowitt SM, Bush K (2014) An assessment of portable X-ray fluorescence spectroscopy in mineral exploration, Kurnalpi Terrane, Eastern Goldfields Superterrane. West Aust Appl Earth Sci 123(3):150–163. https://doi.org/10.1179/1743275814Y.0000000052
42. European Standard EN-ISO 13196:2015, Soil quality - Screening soils for selected elements by energy-dispersive X-ray fluorescence spectrometry using a handheld or portable instrument (ISO 13196:2013, IDT)
43. Marashdeh MW, Bauk S, Tajuddin AA, Hashim R (2012) Measurement of mass attenuation coefficients of Rhizophora spp. binderless particleboards in the 16.59–25.26 keV photon energy range and their density profile using x-ray computed tomography. Appl Radiat Isot 70(4):656–662. https://doi.org/10.1016/j.apradiso.2012.01.008
44. Kurudirek M, Türkmen İ, Özdemir Y (2009) A study of photon interaction in some building materials: high-volume admixture of blast furnace slag into Portland cement. Radiat Phys Chem 78(9):751–759. https://doi.org/10.1016/j.radphyschem.2009.03.070
45. Parsons C, Grabulosa EM, Pili E, Floor GH, Roman-Ross G, Charlet L (2013) Quantification of trace arsenic in soils by field-portable X-ray fluorescence spectrometry: considerations for sample preparation and measurement conditions. J Hazard Mater 262:1213–1222. https://doi.org/10.1016/j.jhazmat.2012.07.001
46. European Standard EN 197–1:2011 Cement - Part 1: Composition, specifications and conformity criteria for common cements, CEN
47. Bourke A, Ross PS (2016) Portable X-ray fluorescence measurements on exploration drill-cores: comparing performance on unprepared cores and powders for 'whole-rock'analysis. Geochem Explor Environ Anal 16(2):147–157. https://doi.org/10.1144/geochem2014-326
48. Ross PS, Bourke A, Fresia B (2014) Improving lithological discrimination in exploration drill-cores using portable X-ray fluorescence measurements:(1) testing three Olympus Innov-X analysers on unprepared cores. Geochem Explor Environ Anal 14(2):171–185. https://doi.org/10.1144/geochem2012-163
49. Ingham J (2019) Geomaterials under the microscope: a colour guide. CRC Press, Boca Raton. https://doi.org/10.1016/C2012-0-01197-0 (**ISBN 978-0-12-407230-5**)
50. European Standard EN 206: 2013 Concrete - Specification, performance, production and conformity, CEN
51. European Standard EN 12620:2002+A1:2008, Aggregates for concrete, CEN
52. Taylor HFW (1997) Cement chemistry, 2nd edn. Thomas Telford Publishing, London, p 459
53. Fort R, Chapa T, González Reyero S (2019) Selective use of limestone in Iberian Iron Age sculptures and monuments: a case study from Jutia (Albacete, Spain). Archaeol Anthropol Sci 11(3):853–870. https://doi.org/10.1007/s12520-017-0574-6
54. Ballesteros D, Painchault A, Puente-Berdasco B, Nehme C, Todisco D, García-Alonso JI, Varano M, Mouralis D (2022) Sourcing of chalkstone used in medieval buildings in the

Eastern Duchy of Normandy (10th− 14th centuries) through geological and geochemistry analyses. Geoarchaeology 37(3):497–521. https://doi.org/10.1002/gea.21907
55. Desroches D, Bédard LP, Lemieux S, Esbensen KH (2018) Suitability of using a handheld XRF for quality control of quartz in an industrial setting. Miner Eng 126:36–43. https://doi.org/10.1016/j.mineng.2018.06.016
56. Desroches D, Bédard LP, Lemieux S, Esbensen KH (2019) Representative sampling and use of HHXRF to characterize lot and sample quality of quartzite at a pyrometallurgical ferrosilicon plant. Miner Eng 141:105852. https://doi.org/10.1016/j.mineng.2019.105852
57. Kasztovszky Z, Maróti B, Harsányi I, Párkányi D, Szilágyi V (2018) A comparative study of PGAA and portable XRF used for non-destructive provenancing archaeological obsidian. Quat Int 468:179–189. https://doi.org/10.1016/j.quaint.2017.08.004
58. Pacheco J, Çopuroğlu O (2016) Quantitative energy-dispersive X-ray microanalysis of chlorine in cement paste. J Mater Civ Eng 28(1):04015065. https://doi.org/10.1061/(ASCE)MT.1943-5533.0001336
59. Potts PJ, Williams-Thorpe O, Webb PC (1997) The bulk analysis of silicate rocks by portable X-ray fluorescence: effect of sample mineralogy in relation to the size of the excited volume. Geostand Newsl 21(1):29–41. https://doi.org/10.1111/j.1751-908X.1997.tb00529.x
60. McNulty BA, Fox N, Berry RF, Gemmell JB (2018) Lithological discrimination of altered volcanic rocks based on systematic portable X-ray fluorescence analysis of drill core at the Myra Falls VHMS deposit, Canada. J Geochem Explor 193:1–21. https://doi.org/10.1016/j.gexplo.2018.06.005